Petroleum Science 20 (2023) 322–336

Contents lists available at ScienceDirect

Petroleum Science

journal homepage: www.keaipublishing.com/en/journals/petroleum-science

Original Paper

Countercurrent imbibition in low-permeability porous media: Non-diffusive behavior and implications in tight oil recovery

Song-Chao Qi [a], Hai-Yang Yu [a, *], Xiao-Bing Han [a], Hang Xu [a], Tian-Bo Liang [a], Xu Jin [b], Xue-Feng Qu [c], Yu-Jing Du [d], Ke Xu [e, **]

[a] State Key Laboratory of Petroleum Resources and Prospecting, China University of Petroleum (Beijing), Beijing, 102249, China
[b] Research Institute of Petroleum Exploration and Development, China National Petroleum Corporation, Beijing, 100083, China
[c] Research Institute of Exploration and Development, PetroChina Changqing Oilfield Company, Xi'an, 710018, Shaanxi, China
[d] School of Engineering and Applied Sciences, Harvard University, Massachusetts, 02138, United States
[e] College of Engineering, Peking University, Beijing, 100871, China

ARTICLE INFO

Article history:
Received 8 June 2022
Received in revised form
28 October 2022
Accepted 30 October 2022
Available online 2 November 2022

Edited by Yan-Hua Sun

Keywords:
Countercurrent spontaneous imbibition
Tight reservoir
Imbibition mechanism
Tight oil development

ABSTRACT

Countercurrent imbibition is an important mechanism for tight oil recovery, that is, water imbibes spontaneously from the fracture into the porous matrix while oil flows reversely into the fracture. Its significance over cocurrent imbibition and forced imbibition is highlighted when permeability reduces. We used the computed tomography (CT) scanning to measure the one-dimensional evolution of water saturation profile and countercurrent imbibition distance (CID) at different fluid pressures, initial water saturations, and permeability. Surprisingly, experiments show that CID evolution for tight reservoir cores dramatically deviates from the classical diffusive rule (i.e., evolutes proportional to square root of time, $t^{0.5}$). At early stage, CID extends faster than $t^{0.5}$ (super-diffusive); while at late stage, CID extends much slower than $t^{0.5}$ (sub-diffusive). After tens of hours, the CID change becomes too slow to be practically efficient for tight oil recovery. This research demonstrates that this deviation from classic theory is a result of (1) a much longer characteristic capillary length than effective invasion depth, which eliminates full development of a classical displacement front; and (2) non-zero flow at low water saturation, which was always neglected for conventional reservoir and is amplified in sub-mili-Darcy rocks. To well depict the details of the imbibition front in this situation, we introduce non-zero wetting phase fluidity at low saturation into classical countercurrent imbibition model and conduct numerical simulations, which successfully rationalizes the non-diffusive behavior and fits experimental data. Our data and theory imply an optimum soaking time in tight oil recovery by countercurrent imbibition, beyond which increasing exposed fracture surface area becomes a more efficient enhanced oil recovery (EOR) strategy than soaking for longer time.

1. Introduction

Tight oil has become a recent hotspot of unconventional oil and gas exploration and development, with the expected production potential of 58 × 10^8 t (U.S. Energy Information Administration, 2018, 2019). The tight oil reservoirs are of low initial oil production, rapid production decline, and commonly low recovery of less than 10% (Cao et al., 2022; Wang et al., 2019; Wei et al., 2021), as a result of low permeability (gas permeability less than 1mD) (Zou et al., 2017). Long horizontal wells and multi-stage volumetric fracturing techniques are conducted to enhance tight formation oil recovery, but it faces the challenge of preferential flow along with the fractures which may leave oil in porous matrix behind and thus result in low oil recovery (Tang et al., 2022; Yu et al., 2019a, 2019b). One solution to improve the sweep efficiency is to make use of the strong capillary pressure caused by small pore size in tight oil reservoirs, to drive spontaneous countercurrent imbibition (Seyyedi and Sohrabi, 2015; Wang et al., 2018; Gruener and Huber, 2019; Yang et al., 2016).

* Corresponding author.
** Corresponding author.
E-mail addresses: haiyangyu.cup@139.com (H.-Y. Yu), kexu1989@pku.edu.cn (K. Xu).

https://doi.org/10.1016/j.petsci.2022.10.022

Nomenclature

C_{spread}	The factor determined by the shape of pore size distribution, dimensionless
D_m	The factor determined by the shape of pore size distribution, dimensionless
D_m	The maximum of diffusion coefficient, mm^2/s
k	Absolute permeability, μm^2 or D
K_{rw} (K_{ro})	Relative permeability of water (oil), dimensionless
P_c	Capillary pressure, MPa
P_o (P_w)	Oil phase (water phase) pressure, MPa
R_o	Imbibition recovery factor, dimensionless
S	Normalized saturation, dimensionless
S_{max}	Maximum water saturation, dimensionless
S_o	Oil saturation, dimensionless
S_{wf}	Wetting phase saturation behind the front, dimensionless
S_{wi}	Initial water saturation, dimensionless
$S_w(x)$	Distribution function of water saturation
V_{im}	The volume of imbibition fluid, cm^3
V_o	The volume of initial oil, cm^3
X_f	Water saturation front (imbibition distance), cm
L	Core length, cm
μ_o (μ_w)	Viscosity of oil (water), mPa s
λ_x	Fluidity of x phase, $\mu m^2/(mPa\ s)$
σ	Interfacial tension, mN/m
ϕ	Porosity, dimensionless

Countercurrent imbibition is the process of displacing the non-wetting fluid by the wetting fluid driven by capillary pressure, that wetting fluid imbibes spontaneously from the open surface (such as fracture) into the porous matrix while non-wetting fluid flows reversely out of the open surface. The classic mechanism of oil-water imbibition indicates that capillary pressure is the main driving force of plane imbibition for sandstone reservoir, which is principally affected by pore radius (Yu et al., 2021; Lu et al., 2022), wettability (Wang et al., 2011; Hou et al., 2022), interfacial tension (Song et al., 2021). Many experimental and theoretical approaches on countercurrent imbibition process have been made (Pooladi-Darvish and Firoozabadi, 2000; Hatiboglu and Babadagli, 2008; Jabbari et al., 2017; Xu et al., 2021). Most of the existing studies focus on evaluating imbibition recovery and analyzing the influence of various factors such as gravity, wettability, oil viscosity, and permeability on imbibition recovery (Tian et al., 2021; Hatiboglu and Babadagli, 2007; Meng et al., 2019b; Polat, 2021). However, countercurrent imbibition in the tight reservoir is too slow due to very low permeability, that water can only penetrate into a limited depth from the fracture during operation time, while leaving oil beyond that depth unaffected. In this scenario, countercurrent imbibition distance (CID) (Meng et al., 2017), defined as the distance between inlet and imbibition front (Fig. 1), is more intuitive to evaluate imbibition efficiency than oil recovery.

Theories have been established for countercurrent imbibition process, and researchers have established analytical solutions (Kashchiev and Firoozabadi, 2003; Schmid et al., 2016), semi-analytical solutions (Deng and King, 2019; Velasco-Lozano and Balhoff, 2021) and numerical models (Yang et al., 2019). Classical oil-water countercurrent imbibition theory predicts that countercurrent imbibition volume and the distance of imbibition front are proportional to the square root of imbibition time (Reis and Cil, 1993), as:

$$CID = \sqrt{D_m t} \tag{1}$$

where CID is the countercurrent imbibition distance; D_m is a constant. Numerous researches have been conducted to correct D_m (Zhang et al., 1996; Fischer et al., 2008; Mason et al., 2010; Hatiboglu and Babadagli, 2010; Standnes and Andersen, 2017; Zhou et al., 2002; Meng et al., 2019a). Some scholars propose that early imbibition recovery deviates from the classical model (Silin and Patzek, 2004; Føyen et al., 2019). Silin and Patzek (2004) extended the countercurrent imbibition model based on Barenblatt's two-phase flow theory of non-equilibrium and predicted that the early stage of imbibition is faster than the square-root law while the late stage converges back to classical square-root law, due to relaxation (Barenblatt, 1971; Barenblatt and Vinnichenko, 1980) caused by water saturation and capillary pressure.

Experimentally, Eq. (1) has also been validated and extended, through indirect measurement or direct recording of detailed saturation profiles. Yang, Z. et al. (2019) estimated the sweeping effect of countercurrent imbibition by high-pressure large-model physical simulation system. However, this experimental method cannot obtain saturation profile, and only the outcrop samples (0.2 and 2mD) were used to study CID. Mirzaei et al. (2016) performed surfactant flooding into oil-wet fractured cores and monitored their imbibition process by CT scanning, and obtained saturation evolution of imbibition under considering gravity. Experimental principles and methods in this literature are similar to our experimental study, but research object is relatively high-permeability cores (250 mD).

There are still very few research that investigate saturation profile evolution and seepage mechanism during countercurrent imbibition in low-permeability (<1 mD) porous media. Recently, Liu and Sheng (2020) conducted nuclear magnetic resonance (NMR) test to investigate evolution of CID during surfactant-enhanced countercurrent imbibition. Although this study focuses more on interpreting the role of surfactant rather than on investigating seepage mechanism, it extends direct record of saturation profile during countercurrent imbibition into < 1mD low-permeability porous media.

The objective of this paper is to experimentally measure

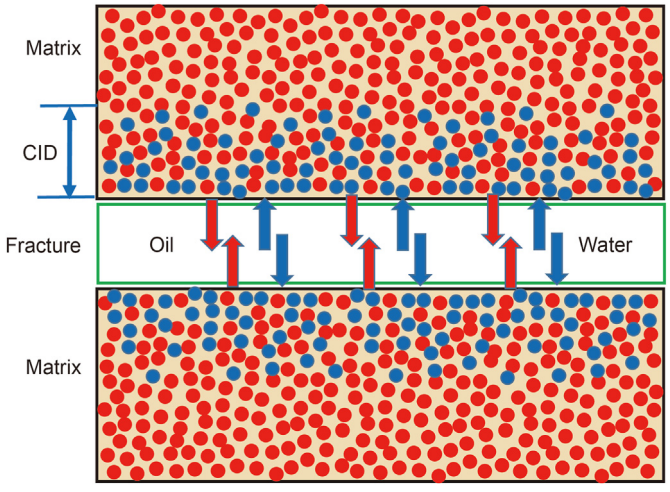

Fig. 1. Schematic diagram of countercurrent imbibition process and CID.

saturation profile and CID evolution during countercurrent imbibition of brine into oil-saturated tight sandstone cores, using CT scanning method. The influences of fluid pressure, water saturation and core permeability on CID are investigated. New scaling during imbibition is observed, and explained by modifying classic imbibition theory at the low-permeability and high-capillarity extreme. This study provides a theoretical basis for practical evaluation of imbibition effect and the development of tight oil reservoirs.

2. Experimental materials and methods

2.1. Core samples

Tight sandstone core samples used in this study were taken from Block A of Changqing Oilfield in the Ordos Basin, China, where the tight oil formation is located around 2570 m underground. The core is set to be horizontal, and the core orientation is consistent with the horizontal stratigraphy direction. By using Porosity Measuring Device and PDP-200 Permeability Measuring Device, porosity was measured according to the principle of gas expansion (i.e. Boyle's law), and permeability was measured by non-steady pressure pulse decay method. In order to make the data more reliable, the porosity and permeability were measured multiple times, and the properties of these cores are given in Table 1. The mineral composition of experimental samples was measured by X-ray diffraction (XRD) analysis as shown in Table 2.

To avoid the influence of pore structure characteristics, the NMR method was used to select cores with similar pore distribution for CID identification. The NMR results of four selected cores show very similar double-peak feature. The shapes and positions of the double-peaks in the four T_2 curves are similar. T_2 relaxation time and the pore size are theoretically correlated, that is, the longer the relaxation time, the larger the pore. The distribution of pores can therefore be judged by the curve distribution and the area under the curve. Through quantitative analysis, the area proportion of left peak (smaller pore) of cores A-1, A-2 and A-3 are 72.96%–73.87%, and the area proportion of right peak (larger pore) are 26.13%–27.08%, and the overall T_2 curve distribution is close, indicating that the three cores have similar pore structure. The T_2 amplitude value of core A-4 with higher permeability is greater than that of the other three cores. Finally, three cores with similar permeability and pore distribution and a core with higher permeability were selected for this study. The results of the NMR experiments of cores are shown in Fig. 2.

2.2. Fluids and core wettability

The crude oil used in this study was taken from the same field. The oil components, measured by the Agilent 7890A gas chromatograph, are shown in Fig. 3a. At the temperature of 25 °C and atmospheric pressure, the oil viscosity is 15 mPa s and the density is 0.79 g/cm^3. The total salinity of the formation water is 49779 mg/L, and the components and properties of formation water are shown in Table 3. In this experiment, the artificial formation water was prepared according to its ionic composition and salinity, and water viscosity is 1.03 mPa s at 25 °C.

The core wettability was characterized by contact angle of oil on smoothed core sample surface in water environment using JY-PHB contact angle equipment before imbibition experiment, following the procedures of petroleum standard SY/T 5153-2017: (1) core sample with smoothed surface, as well as the measuring chamber, are thoroughly cleaned; (2) core sample is put into the measuring chamber, and the measuring chamber is filled with formation water and soaked for 48 h; (3) the oil droplet is injected under the core sample by using a micro-syringe, and balanced for 168 h; (4) then final contact angle is determined when the contact angle remained unchanged. As shown in Fig. 3b (for A-1 core), the core is water-wet.

2.3. Experimental procedures

X-CT scanning experiment is performed to measure CID, and the experimental instrument and data processing are shown in Appendix-A. The effects of fluid pressure, water saturation and core permeability on CID are further investigated. This experiment studies the countercurrent imbibition process where the injected fluid contacts with flat rock end-face. The cores are sealed by epoxy resin except for the inlet, and the injected fluid only contacts with the inlet of cores, so there is no displacement pressure difference. In the imbibition process, the injected fluid is imbibed into the core, and crude oil in the core is expelled. The CID increases with time, then imbibition is considered to over when CID hardly changes. Some experimental parameters such as pressure and initial water saturation are designed with reference to the reservoir conditions of target block, and the schematic diagram of countercurrent imbibition process is shown in Fig. 4. The specific procedures are as follows:

(1) The CT values of air, crude oil and simulated formation water are measured under the condition of scanning current of 160 mA and scanning voltage of 120 kV, at experimental pressure and ambient temperature (25 °C).
(2) Experimental cores are cleaned with organic solvent for 14 days, referring to the relevant regulations of petroleum industry standard SY/T 5336-2006. The cleaned cores are dried at 100 °C in a drying apparatus for 2 days, then taken out and placed in a desiccator for cooling.
(3) Select a dry core and put it in the core holder, and pressurize it to experimental confining pressure and backpressure, then vacuum it to the steady state (the pressure has no obvious change within 2 h). Measure the CT value of each cross-section of the dry core (the scanning layer thickness is 1.25 mm, and the scanning interval is 5 mm).
(4) To avoid the influence of live oil degassing, dead oil is used to saturate tight cores. The core is vacuumed for 7 days to the steady state and saturated with crude oil at 20 MPa for 21 days. Then, the core saturated with oil is aged for 7 days for subsequent experiments. The core saturated with crude oil is scanned to measure the CT value of each cross-section.
(5) Close the outlet valve, then use the injection pump to pressurize water at the inlet. Confining pressure is always set to be 3 MPa higher than inlet pressure. When the inlet reaches

Table 1
The properties of experimental cores.

Sample	Length, cm	Diameter, cm	Pore volume, cm^3	Gas permeability, mD	Porosity, %
A-1	5.046	2.509	2.230	0.311 ± 0.003	8.94 ± 0.02
A-2	5.051	2.492	2.156	0.314 ± 0.001	8.75 ± 0.01
A-3	5.037	2.489	2.159	0.312 ± 0.002	8.81 ± 0.02
A-4	5.043	2.496	2.727	0.796 ± 0.002	11.05 ± 0.03

Table 2
XRD analysis results of core samples.

Mineral composition, %						Clay minerals analysis, %				
Quartz	Feldspar	Dolomite	Calcite	Pyrite	Clay	S	I	I/S	C	K
51.5	29.7	4.1	3.5	–	11.2	–	34.4	23.3	42.3	–

Note: S: Smectite; I: Illite; C: Chlorite; K: Kaolinite; I/S: Illite/smectite mixture.

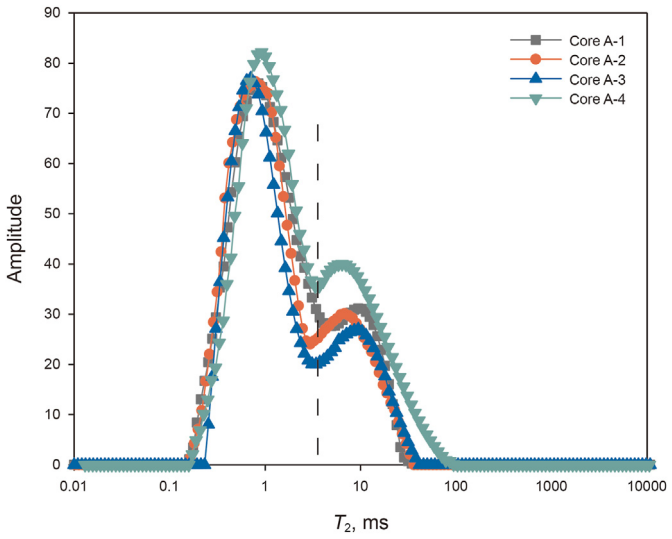

Fig. 2. The results of NMR experiments of cores.

the target pressure, the injection pump automatically shuts down then quickly close the inlet valve. The back pressure regulator always monitors whether there is liquid flow at the outlet. At this moment, the imbibition process starts in the sealed core holder (Fig. 4a).

(6) In the early stage of the experiment, CT scanning can be performed every 10 min, and the initial position of each scan should be consistent. In the later stage of the experiment, CT scanning can be performed three times a day. The CID of water is determined by finding the cross-section position where water saturation suddenly becomes zero (Fig. 4b), and there may be the quantization error of a CT scan thickness (1.25 mm) for CID quantification.

When studying the effects of fluid pressure and core permeability on CID, the dry cores are saturated with crude oil in this experiment, and there is no water in the cores. However, in order to study the influence of water saturation on CID, it is necessary to establish the irreducible water saturation of core A-3, then conduct the experiment for measuring the CID.

3. Results

The saturation profiles during countercurrent imbibition under different conditions are shown in Fig. 5. Note that negative water saturation values come from the measurement error of 2%–3%. All experiments show qualitatively similar results: water gradually imbibes from the right side of the core, during which the inlet water saturation increases. Water invasion gradually slows down, and the saturation profile changes very little after about 72 h during these imbibition experiments. We define the CID at 72 h as steady-CID (SCID). The imbibition front does not reach the closed end boundary during the experiment. The oil recovery factor can be calculated from the water saturation profile, as:

$$R_o = \frac{V_{im}}{V_o} = \frac{\int (S_w(x) - S_{wi})dx}{L(1 - S_{wi})} \quad (2)$$

where V_{im} is the volume of imbibition fluid; V_o is the volume of initial oil; L is the core length; $S_w(x)$ is the distribution function of water saturation; S_{wi} is the initial water saturation.

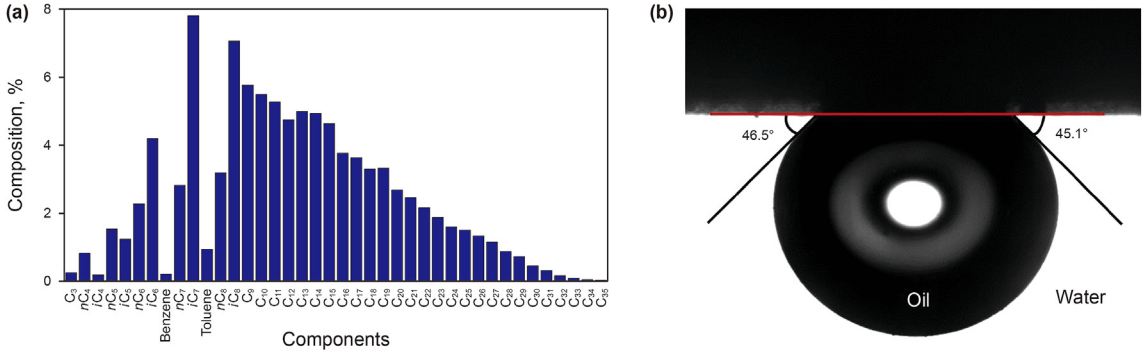

Fig. 3. Test results of fluid and core wettability. (**a**) The components of crude oil; (**b**) Core wettability test results.

Table 3
The components and properties of artificial formation water.

Ion concentration, mg/L						Total salinity, mg/L
$K^+ + Na^+$	Ca^{2+}	Mg^{2+}	Cl^-	SO_4^{2-}	HCO_3^-	
16207	2528	270	29703	734	337	49779

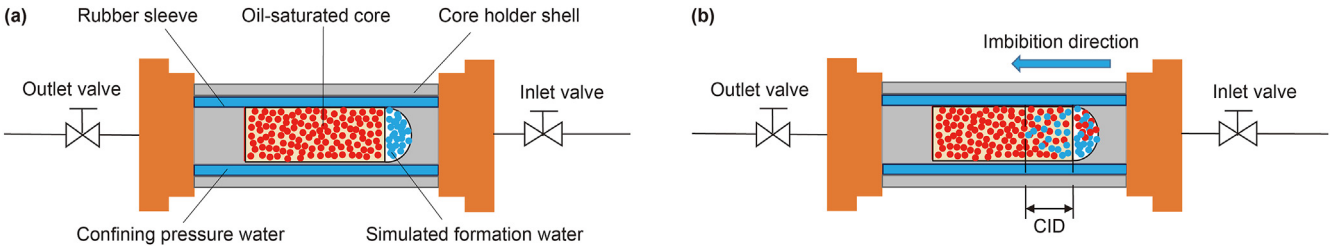

Fig. 4. The schematic diagram of countercurrent imbibition process. (**a**) The initial state of countercurrent imbibition; (**b**) The final state of countercurrent imbibition.

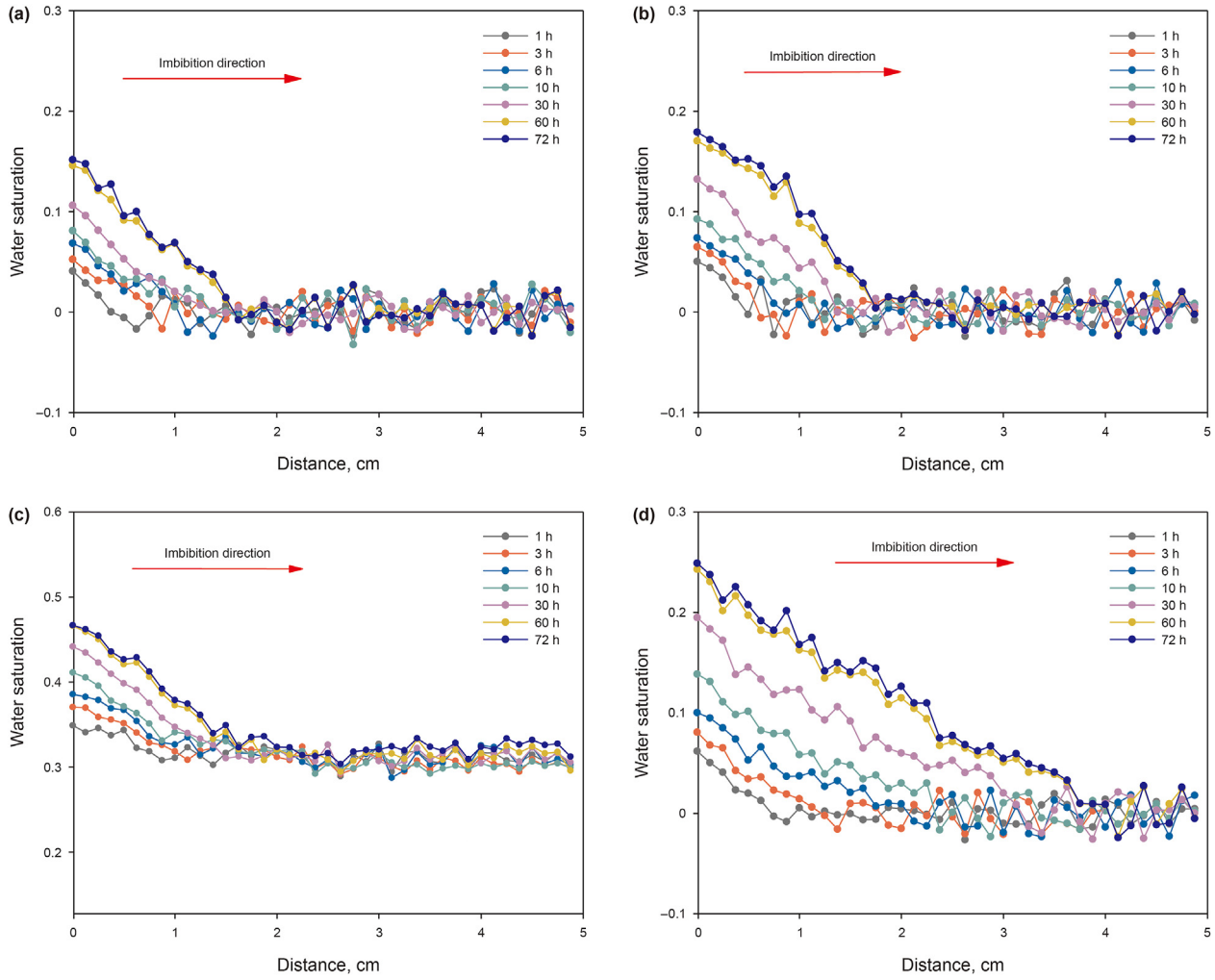

Fig. 5. Experimental results of CID under different experimental conditions. (**a**) Core A-1 under 5 MPa condition; (**b**) Core A-2 under 20 MPa condition; (**c**) Core A-3 with the initial water saturation of 31.66%; (**d**) Core A-4 with a permeability of 0.796 mD.

The evolution of countercurrent imbibition recovery of different cores is thus calculated and presented, as shown in Fig. 6a. Even at the very end of the experiments that water invasion almost terminates, the total oil recovery is only about 2%–3% for cores of permeability of 0.3 mD, and about 9% for core A-4 with higher permeability. If the cores are lengthened by twice during infinite-acting imbibition regime, in the same condition, the actual evolution of water saturation profile has little change and the recovery factor would decrease by about twice (demonstrated in the later section). Oil recovery thus fades more indicative information of how much region is actually influenced by water.

Compared to recovery factor, CID is a more informative indicator of countercurrent imbibition in tight cores. It indicates actual influence range of imbibition, which has been experimentally shown limited near the fracture surface, regardless of the size of unaffected region. CID evolution of four experiments are shown in Fig. 6b, showing a similar trend to the recovery factor. Clearly, invasion slows down after a critical point and changes slightly after 72 h, at which time even the imbibition of higher permeability core (0.796 mD) only influences less than 4 cm in the matrix.

Experiment performed on core A-1 with 0.311 mD is set as a reference. The fluid pressure is set as 5 MPa and the initial water saturation is set as 0%. After 72 h of imbibition, the SCID of core A-1 is 1.375 cm. When the fluid pressure is 20 MPa in the experiment

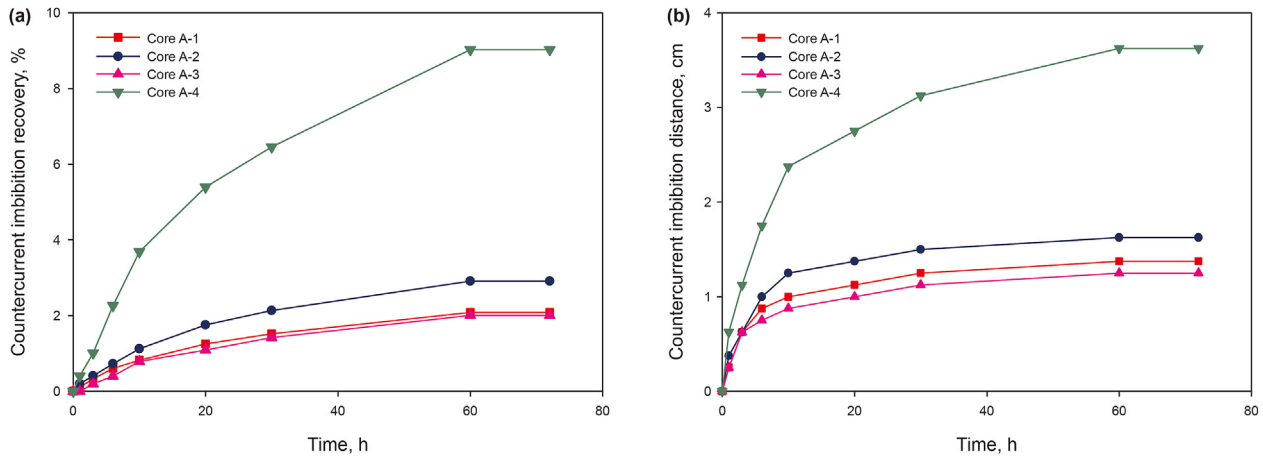

Fig. 6. Evolution process of countercurrent imbibition for different cores. (**a**) Evolution of countercurrent imbibition recovery; (**b**) CID evolution.

using core A-2, SCID (1.625 cm) is only insignificantly larger than that of the reference experiment as a response of expanded pore space. Initial water saturation is set as 31.66% in the experiment using core A-3, which results in a slightly lower SCID (1.25 cm) compared to the reference experiment, which may be interpreted as a reduction of capillary driving force in presence of larger initial water saturation. Permeability is more than doubled in core A-4 (0.796 mD) compared to the reference experiment, and the corresponding SCID is also more than doubled (3.625 cm), showing the dominant influence of permeability on countercurrent imbibition efficiency. Most of important results for the four experiments are shown in Table 4.

We note that, even at the very end of each experiment, the inlet water saturation is still relatively low, without formation of an integrated saturation displacement "front". This is very different from observations using high-permeability or high porosity samples (Bourbiaux and Kalaydjian, 1990; Guen and Kovscek, 2006).

4. Discussion

4.1. Break-down of classical square root models

Surprisingly, experimental data significantly deviates from classic square-root rules, as illustrated by plotting the double logarithmic graph of CID against t for experimental data in Fig. 7: early-stage CID evolves faster than $t^{0.5}$ (super-diffusive), while late-stage CID increases much slower than $t^{0.5}$ (sub-diffusive). Although some work proposed early-stage fast imbibition with super-diffusive scaling, such as Silin and Patzek (2004), no theory is found that can explain both the early super-diffusive stage and the late sub-diffusive stage. This deviation from classic square root model is also illustrated in CID–$t^{0.5}$ plot, as shown in Fig. 8: in the early stage, the curve is downwardly convex; in the late stage, the curve is upwardly convex. When using $t^{0.75}$ as the x-axis, the linearity of the early stage appears much better.

In addition, we investigated relevant experimental research in literature. Due to the differences in experimental purpose, experimental core types, permeability, etc., few experimental studies are available to compare with our results of countercurrent imbibition in <1 mD cores. Nevertheless, we note that Liu and Sheng (2020) conducted NMR test and obtained the water saturation profiles in tight cores during countercurrent imbibition, which can be used for analogy with our experimental research. In this work, we also note the emergence of two countercurrent imbibition stages, with clear sub-diffusive (later stage) and suspected super-diffusive (early stage). Regrettably, their early-time data are so sparse and few that more convincing analysis is not applicable. Discussion and analysis are shown in Appendix C.

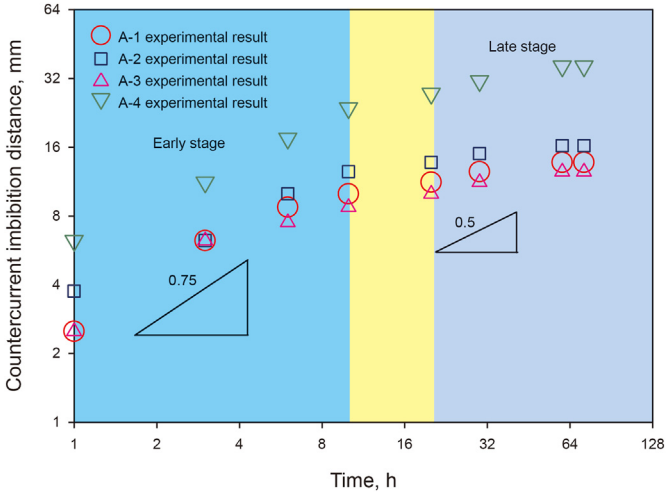

Fig. 7. Double logarithmic graph of CID and time for experimental data (Black triangle is an auxiliary line with a slope of 0.75 and 0.5).

Table 4
Experimental results of SCID under different experimental conditions.

Sample	Fluid pressure, MPa	Initial water saturation, %	SCID, cm	Dimensionless CID	Water saturation of inlet, %
A-1	5	0	1.375	0.272	15.16
A-2	20	0	1.625	0.322	17.92
A-3	5	31.66	1.250	0.248	46.88
A-4	5	0	3.625	0.719	24.89

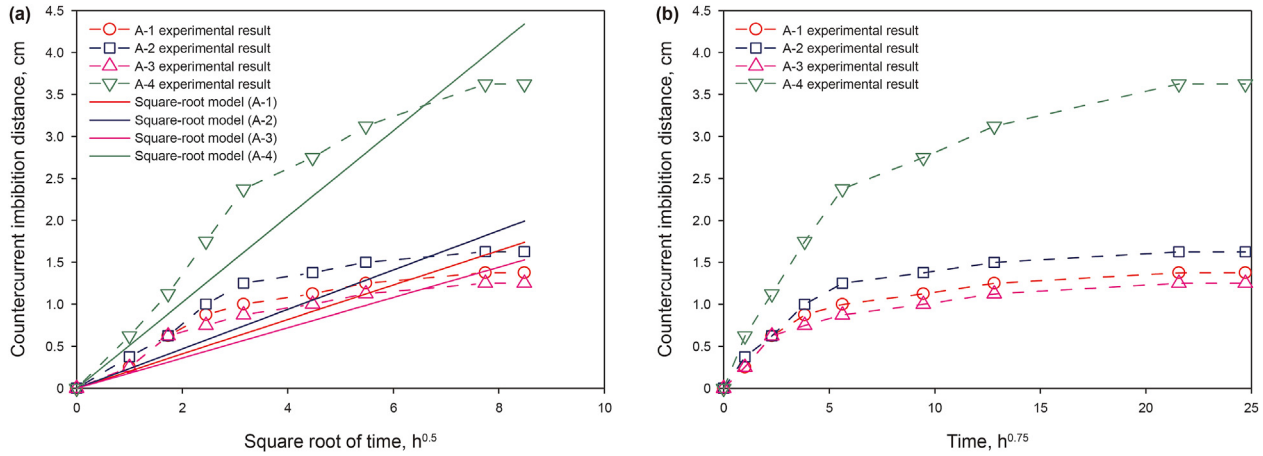

Fig. 8. (**a**) Comparison between classic square-root model and experimental results using $t^{0.5}$ as the *x*-axis, and the solid lines are fitted lines using square root rule. Note that the early stage data in every set of data are clearly downward-convex; (**b**) Re-plot of the CID–time data with $t^{0.75}$ as the *x*-axis. Note that the linearity of early time becomes much better.

4.2. Analysis of non-diffusive countercurrent imbibition

In order to explain this deviation from the square-root rule while to avoid complex numerical simulation, we re-visit classical square-root model (Reis and Cil, 1993; Li et al., 2003; Mason et al., 2009), where the CID is derived as:

$$X_f = \sqrt{D_m t} = \sqrt{\sqrt{\frac{2k}{\varphi}}\frac{C_{spread}\sigma}{\left(S_{wf}-S_{wi}\right)\left(\mu_w/K_{rw}+\mu_o/K_{ro}\right)}t} \tag{3}$$

where X_f is the water saturation front; k is absolute permeability of cores; C_{spread} is the factor determined by the shape of pore size distribution; σ is the interfacial tension; S_{wf} is the wetting phase saturation behind the front; μ_w is the viscosity of water; μ_o is the viscosity of oil; K_{rw} is the relative permeability of water; K_{ro} is the relative permeability of oil; t is the imbibition time.

We note that the classical square-root model assumes the pre-coefficient of time constant. It is a valid assumption if the displacement front is well-developed and the length of saturation transition zone (the front thickness) is negligible, so only two saturation values exist: the mainly oil-saturated zone ahead of the front, and the mainly water-saturated zone behind it (Li et al., 2003; Mason et al., 2009). However, according to the capillary pressure experiment and other data, the capillary pressure is so dominant that abovementioned assumption may not be valid. We can estimate the length of saturation transition zone (capillary length) as $L_c = kA\Delta P_c/q_\mu$ based on Darcy's law (Hammecker et al., 1993; Masalmeh et al., 2007), which is ~350 cm for core A-1. This value of capillary length is two orders of magnitudes larger than the core length. As a consequence, in low-permeability porous media like these applied in the experiment, the displacement front is far from being fully developed, which breaks the "negligible front length" assumption. Two constant-saturation zones no longer exist, and we need to look into the details of this "incomplete front", or "capillary transition zone", in order to rationalize this breakdown of classic diffusive model.

We thus revisit the derivation of countercurrent imbibition. The flux for both liquids can be written as:

$$q = q_w = -\lambda_w^*\nabla P_w = -\lambda_w^*(\nabla P_o - \nabla P_c) \tag{4}$$

$$-q = q_o = -\lambda_o^*\nabla P_o \tag{5}$$

with

$$\lambda_x^* = A\lambda_x = Ak\frac{k_{rx}}{\mu_x}$$

$$\nabla P_w = \frac{\partial P_w}{\partial x}$$

$$P_c = P_o - P_w$$

Summating Eqs. (4) and (5) yields:

$$(\lambda_o^* + \lambda_w^*)\nabla P_o = \lambda_w^*\nabla P_c \tag{6}$$

Substituting Eq. (5) into Eq. (6) yields:

$$q = \left(\frac{1}{\lambda_w^*}+\frac{1}{\lambda_o^*}\right)^{-1}\frac{dP_c}{dS_w}\cdot\nabla S_w \Rightarrow \nabla q = \nabla\cdot\left(\left(\frac{1}{\lambda_w^*}+\frac{1}{\lambda_o^*}\right)^{-1}\frac{dP_c}{dS_w}\cdot\nabla S_w\right) \tag{7}$$

One can cast the continuity equation $A\phi\frac{\partial S_w}{\partial t}+\nabla q = 0$ into a nonlinear diffusion equation:

$$\frac{\partial S_w}{\partial t} = \nabla\cdot\{F(S_w)\nabla S_w\} \tag{8}$$

with

$$\nabla\cdot\{F(S_w)\nabla S_w\} = \frac{\partial\left\{\left(F(S_w)\frac{\partial S_w}{\partial x}\right)\right\}}{\partial x}$$

$$F(S_w) = \frac{1}{\phi}\left(\frac{1}{\lambda_w}+\frac{1}{\lambda_o}\right)^{-1}\left(-\frac{dP_c}{dS_w}\right) > 0$$

Referring to the mathematical and physical discussion of Vazquez (2006) and Lukyanov et al. (2012), the characteristics of this diffusion equation depend on nonlinear type dictated by the $F(S_w)$ term. If $\frac{dF}{dx} = \frac{dF}{dS_w}\cdot\frac{\partial S_w}{\partial x} > 0$, CID evolves faster than $t^{0.5}$. If $\frac{dF}{dx} = \frac{dF}{dS_w}\cdot\frac{\partial S_w}{\partial x} < 0$, CID envolves slower than $t^{0.5}$. Only when $dF/dx = 0$, the CID evolves in a diffusive way that CID $\propto t^{0.5}$ rigorously holds.

The expression of $F(S_w)$ indicates that CID evolution is controlled

by fluidity term $(1/\lambda_w + 1/\lambda_o)^{-1}$ and capillary pressure term $-\mathrm{d}P_c/\mathrm{d}S_w$, both of which are functions of water saturation, S_w. By assuming that fluidity of water is zero at and below S_{wi}, McWhorter and Sunada (1990) and Kashchiev and Firoozabadi (2003) obtained a typical diffusion function (i.e. $F(S_w)$) as a bell-shaped curve through the typical capillary pressure and relative permeability equations proposed by Brooks-Corey, and $F(S_w)$ is the maximum at S_m.

However, the fluidity of wetting phase has shown not exactly zero at and below S_{wi}. Theoretical and experimental study has shown that the initial relative permeability of wetting phase can be approximately regarded as a constant at low water saturation (Lukyanov et al., 2012). This non-zero fluidity for wetting phase at low saturation is attributed to the presence of grain surface roughness, corner flow and microporosity (Bonn et al., 2009; Liu et al., 2014; Quere, 2008; Kim et al., 2021). Although it has long been noticed, classic modeling in porous media generally neglect it, as it is so sensitive to specific surface area and in high-permeability case that specific surface area is relatively low. However, the non-zero fluidity along surface roughness and conner should be highlighted in low-permeability scenario that the specific area is highly amplified. Therefore, classical relative permeability equations are modified to include this non-zero water fluidity term at low water saturation, as shown in Eqs. (9) and (10).

$$K_{rw} = a + S^{(2+3b)/b} \tag{9a}$$

$$K_{ro} = (1-S)^2\left(1 - S^{(2+b)/b}\right) \tag{9b}$$

$$P_c = P_0 S^{-1/b} \tag{10}$$

where $S = S_w/S_{max}$ is the normalized saturation, assuming $S_{max} = 1$ for the convenience of data calculation; P_0 is a characteristic capillary pressure; a is the relative permeability of wetting phase when $S_w > 0$; b is a parameter related to the distribution of pore sizes (Brooks and Corey, 1964). We note that both P_0 and b can be directly measured and only the value of a should be obtained by fitting. We plot the fluidity term, capillary pressure term, and $F(S_w)$ as functions of normalized saturation, as shown in Fig. 9.

Under low water saturation, $(1/\lambda_w + 1/\lambda_o)^{-1} \sim \lambda_w$ approximates to a constant, and the increase with S_w is slow. In addition, the capillary pressure term is a monotonically decreasing function according to Eq. (10), with a large gradient under low water saturation, as shown in Fig. 9b. Accordingly, $F(S)$ starts from infinity and gradually decreases at low water saturation, when water saturation grows larger, the increase of fluidity gradually dominates while the decrease of $-\mathrm{d}P_c/\mathrm{d}S$ shows down, which results in the increase of $F(S)$ as predicted by classical bell-shaped curve, as shown in Fig. 9c.

The shape of F can help to explain the two-stage countercurrent imbibition kinetics for low-permeability rocks as we experimentally observed. In the early-stage, water saturation in the invaded region is low, so $\mathrm{d}F/\mathrm{d}S_w < 0$ and $\mathrm{d}F/\mathrm{d}x > 0$, therefore CID increases faster than classic diffusive $t^{0.5}$ law. Specifically, as the mobility of oil, at low water saturation, can be treated as negligible compared to water mobility, the mathematical formula at this early stage is identical to that of Lukyanov et al. (2012), although the latter is co-current imbibition of water to displace air. We therefore directly borrow their conclusion that CID- $t^{0.75}$, which perfectly matches our experimental data as shown in Fig. 7. However, in the late-stage of imbibition, the water saturation gradually increases to a higher value, reverses $\mathrm{d}F/\mathrm{d}S_w$ to be positive, and finally results in CID increases slower than $t^{0.5}$.

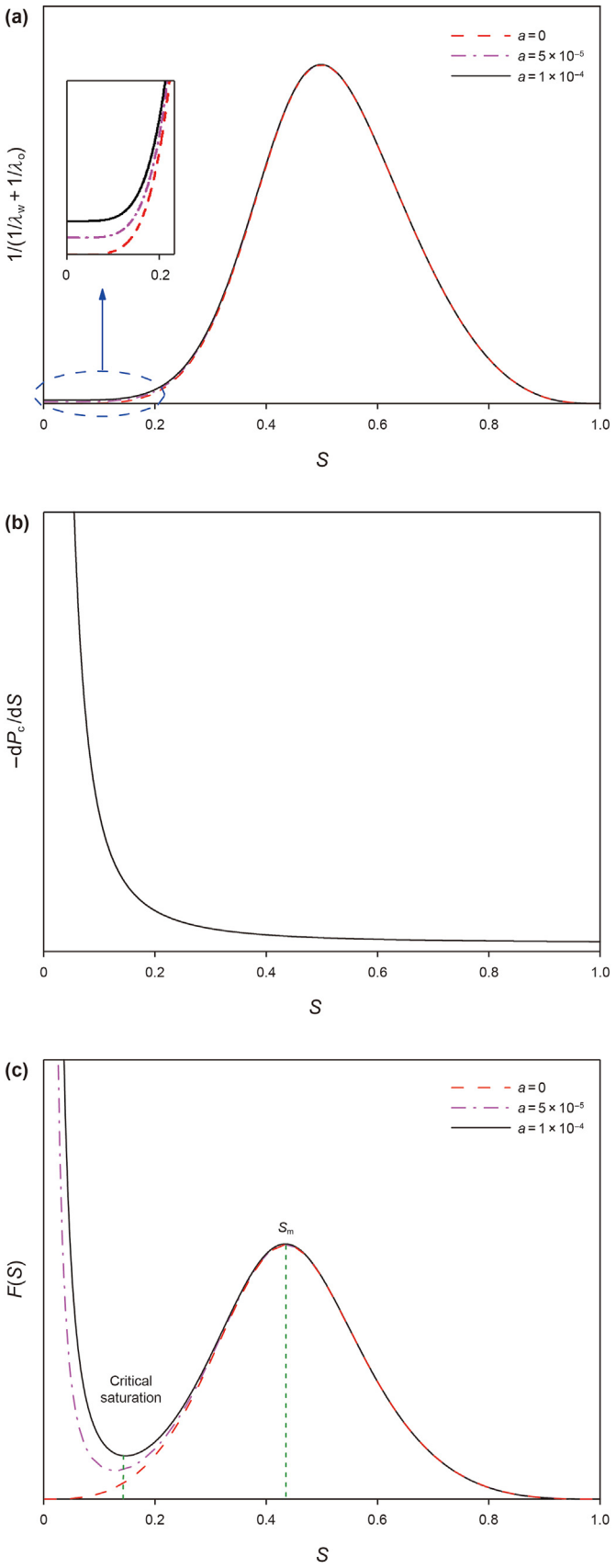

Fig. 9. Function graph when $b = 1$. (**a**) The curve of fluidity term; (**b**) The curve of capillary pressure term; (**c**) The curve of $F(S)$ function.

The above derivation and scaling arguments well explain the experimental observations. It also reveals the physics controlling the transition from super-diffusive and sub-diffusive. When water saturation is below that of the minimum F (i.e. critical saturation), the flow is dominated by that along surface roughness, corners and continuous micropores; when water saturation is above that of the minimum F, the flow is dominated by classic imbibition along the pore bodies. The transition from super-diffusive behavior to sub-diffusive behavior thus marks the transition of flow pattern, from roughness/corner/microporosity flow to classic spontaneous imbibition.

4.3. Model fitting

Based on Eq. (8)-Eq. (10), the numerical solution is performed by using MATLAB programming to simulate countercurrent imbibition process. In this subsection, we first choose results of core A-1 for validation and demonstration, and the fitting parameters and fitting results of the other three cores are shown in Table 5 and Fig. 10. Parameters b and P_0 are obtained from capillary pressure curve (Appendix B). For core A-1, $b = 1.2$ and $P_0 = 0.03$ MPa. Further, by fitting the model against experimental data of water saturation evolution, we determine $a = 8 \times 10^{-5}$, which is in reasonable interval 9.59×10^{-6} –1.1×10^{-4} (Appendix B) (Lukyanov et al., 2012). The fitted curves are surprisingly consistent with the experimental results (Fig. 10a). Simultaneously, the CID fitting results of four simulations also show a consistent evolution law with the experimental results, as shown in Fig. 11. The model fitting in long-hours results is better than the short-hours results, and this is attributed to the larger error at the very beginning. As the error of saturation from CT-scanning measurement is irrelevant to absolute saturation, higher saturation would bring smaller relative error.

A critical water saturation that the evolution of CID transient from super-diffusive to sub-diffusive can be obtained by solving $dF/dS = 0$ and choose the smallest positive solution (the analytical solution for critical saturation is illustrated in Appendix B). Then the critical imbibition time can be obtained. In the case of core A-1 experiment, the critical water saturation is estimated to be 0.118 by solving $dF/dS = 0$. We can then solve the time that the inlet water saturation is 0.118, which yields a critical time of about 29.9 h. This solved time matches with the transition time as shown in Fig. 7.

4.4. Comparison against classic models

In order to describe the early “super-diffusive” imbibition process, the parameter a characterizing the low-saturation no-zero relative permeability is introduced. This is the major difference between our model (modified model) and earlier approaches (McWhorter and Sunada, 1990; Kashchiev and Firoozabadi, 2003). We note that as the parameters P_0 and b can be determined by the experimentally measuring capillary pressure curve, there is only one fitting parameter a.

Taking experiment A-1 as an example, $b = 1.2$ and $P_0 = 0.03$ MPa are obtained by fitting the capillary pressure curve, then parameter a is fitted through imbibition saturation profile: for the modified model $a = 8 \times 10^{-5}$, and for the previous classic model $a = 0$. As shown in the comparison of simulation results (Fig. 12), water saturation profile of previous model is “upwardly convex” shape, which is significantly different from the “downwardly concave” shape of the experimental results, while water saturation profile of modified model is similar to the experimental results and is “downwardly concave”. The modified model is obviously much better to fit experimental results.

Table 5
Fitting parameter results of four core experiments.

Sample	P_0, MPa	a	b
A-1	0.030	8.1×10^{-5}	1.2
A-2	0.038	6.1×10^{-5}	1.3
A-3	0.031	5.4×10^{-5}	1.2
A-4	0.026	9.0×10^{-5}	1.8

4.5. Effect of core length

In order to clarify the influence of the closed outlet boundary on imbibition profile evolution during infinite-acting imbibition regime and observe the relationship between CID and imbibition recovery for long cores, the numerical simulation using our modified model is conducted. The countercurrent imbibition process of 5, 10, and 20 cm cores is simulated. As shown in Fig. 13, the simulation results of 5, 10, and 20 cm cores are similar as a whole: water saturation almost coincides before 30 h, and water saturation at the inlet still almost coincides while water saturation at distal end of longer core rises slightly after 30 h. Therefore, the distance of the closed boundary has little effect on the overall water saturation during infinite-acting imbibition regime.

Although the length of core results in little difference in actual imbibition process, it does affect the calculated recovery factor, as the longer core contains more immobilized oil that results in lower recovery, although actual invasions changes little. It thus echoes our earlier claim that oil recovery may not be an indicative value to characterize the actual imbibition kinetics, and it is not an appropriate base to compare the imbibition efficiency.

It also shows that the countercurrent imbibition is a highly localized process, which further highlights the dominance of countercurrent imbibition over cocurrent imbibition during spontaneous imbibition in low-permeability media. Cocurrent imbibition requires flow through the whole porous media, while countercurrent imbibition only requires flow near the surface exposed to water. For cocurrrent imbibition, flow resistance increases proportionally with $1/k$ and with L; in comparison, for countercurrent imbibition, the flow resistance is proportional to the ratio of CID to k and CID also reduces with decreasing k. As a result, the relative significance of cocurrent imbibition compared to countercurrent imbibition reduces with the decreasing of permeability. When the permeability is low enough, imbibition becomes highly localized and is dominated by countercurrent imbibition, at least in short time-scale.

5. Implications and limitations

The observation and rationalization of non-diffusive countercurrent imbibition in low permeability porous media may provide guidance for enhancing tight oil recovery. The CID is only of the order of centimeters in reasonable time scale, leaving all oil deep in the matrix immobile. Increasing pressure may not be a good stimulation measure for imbibition, but improving reservoir permeability and establishing complex fracture network to increase fracture-matrix contact area may be more effective. More importantly, we show that when the early-stage super-diffusive imbibition is completed, further soaking becomes economically inefficient. Meanwhile, the research results trigger some thoughts for enhancing the imbibition recovery of tight reservoir: (1) whether to use some auxiliary measures can increase the CID and enhance imbibition recovery, and (2) as the increase of CID is limited, creating more fracture surfaces may improve the range of imbibition sweeping more efficiently than simply soaking for longer time.

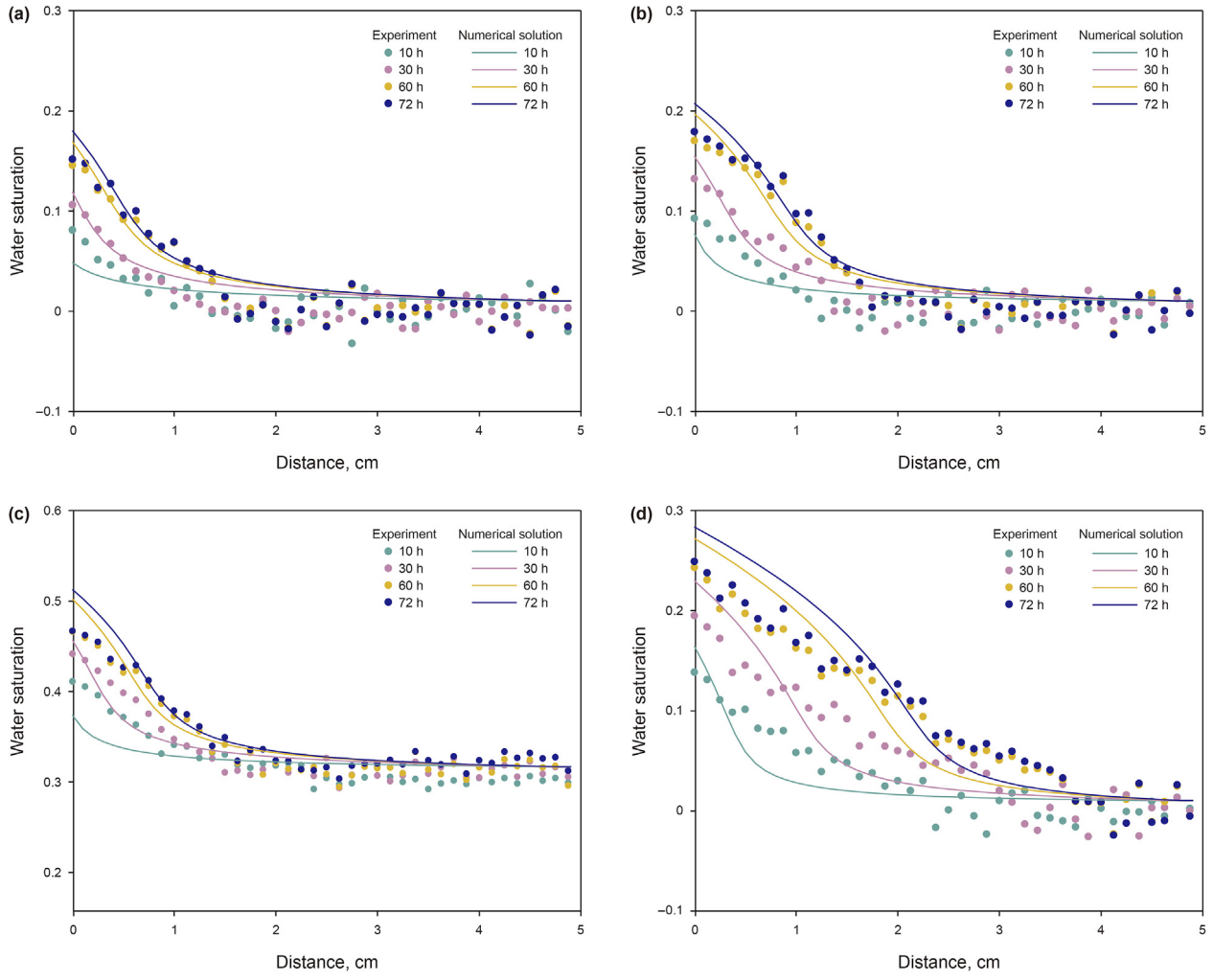

Fig. 10. The one-dimensional numerical solution of saturation distribution.

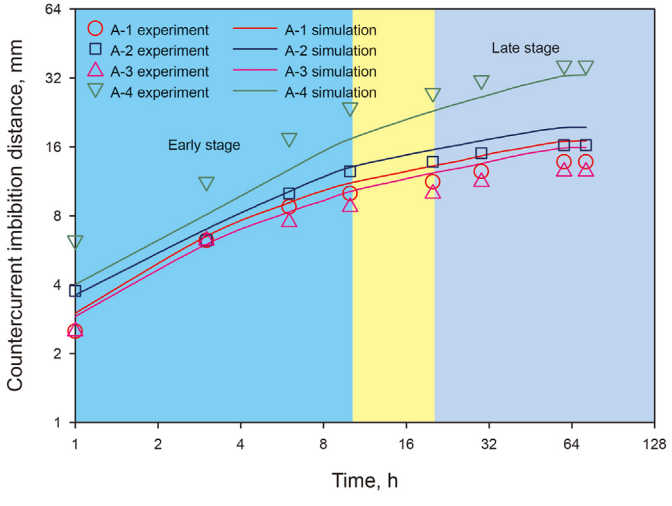

Fig. 11. CID vs. *t* double logarithmic graph of simulation results and experimental results.

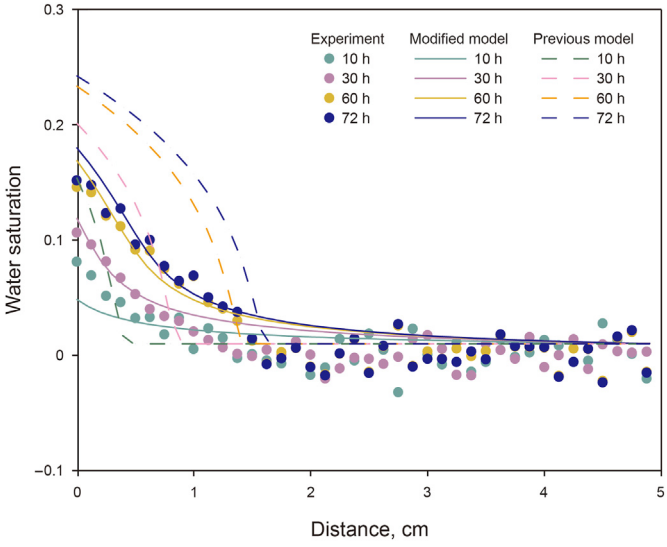

Fig. 12. Fitting comparison of previous classic model and modified model for experimental results of core A-1.

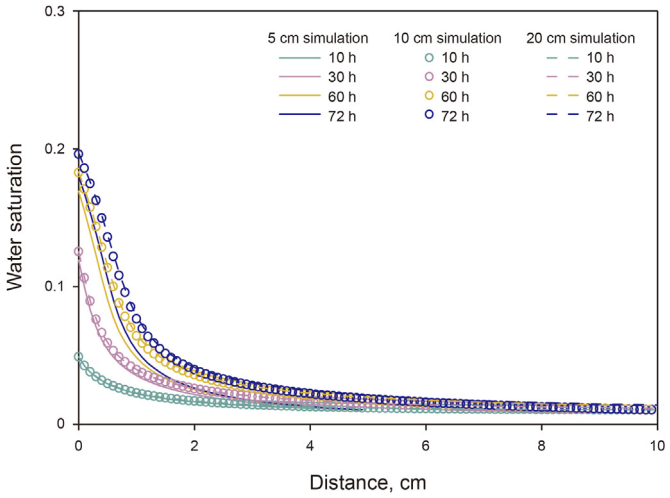

Fig. 13. Comparison of simulation results for 5, 10, and 20 cm cores.

CID is a direct quantification of imbibition effect distance. In linear 1-D system, the ratio of CID over total length is the sweep efficiency. In 3-D systems, the product of CID and total surface area exposed to water is the total swept volume. Given the area of fracture, the sweep efficiency can be easily calculated. In addition, we note that there is inconsistent definition of "tight rock" around the world (Meng et al., 2018). Nonetheless, the discovery in this work is not affected by such definitions. The analysis into capillary transition zone and the fluidity at low water saturation should be conducted as long as the rock is water-wet and the permeability is low enough that the capillary length is not negligible.

The mineral composition of cores used in experiments is mainly quartz and feldspar, both of which are stable in properties and do not reaction with brine. Clay mineral is an integral part of the reservoir rock as a cementing material, and the clay content of experimental core is low, so the effect of osmotic pressure can be ignored. Osmotic pressure and chemical reaction are not considered in this study.

Nevertheless, further exploration of countercurrent imbibition at lower permeability is limited by the capacity of CT instruments. In this preliminary investigation, the interpreted imbibition distance for core permeability less than 0.3 mD is unreliable. Meanwhile, due to the limitation of formation cores, there are not many formation cores with similar core properties to conduct the parallel comparative experiment. Instruments with higher resolution should be applied for further research of countercurrent imbibition in porous media with even lower permeability.

6. Conclusions

In this research, countercurrent imbibition experiments are conducted on tight cores with permeability lower than 1 mD, and CT scanning technology is applied to quantify the evolution of CID (countercurrent imbibition distance). Surprisingly, we find that CID evolution in tight cores does not follow classic diffusive scaling: in early stage, CID increases much faster than ~ $t^{0.5}$; in late stage, CID evolution slows down to be much slower than ~ $t^{0.5}$. As a result, countercurrent imbibition in tight core is more effective in the first stage, and changes slightly in later stage.

This paper reveals the physics that results in this deviating from classic theory, and shows that capillary length in such low-permeability porous media is much larger than the CID, due to the small pore size and large capillary pressure. Consequently, the classic "displacement front" does never fully develop, therefore the classic diffusive scaling fails. By re-deriving the spontaneous countercurrent imbibition dynamics that taking non-zero fluidity of wetting phase at low saturation into consideration, we rationalize the measured super-diffusive fast imbibition at the early stage and the sub-diffusive slow imbibition at later stage. The new theory can fit the experimental data of saturation evolution very well. The emergence of two stages may imply the existence of an optimum soaking time to recover oil from tight formation just by countercurrent imbibition.

Declaration of competing interest

The authors declare the following financial interests/personal relationships which may be considered as potential competing interests: Hai-Yang Yu reports financial support was provided by National Natural Science Foundation of China. Ke Xu reports financial support was provided by National Natural Science Foundation of China. Ke Xu reports was provided by China National Petroleum Corp.

Acknowledgments

This research was financially supported by National Natural Science Foundation of China (No. 52074317), China National Petroleum Corporation-China University of Petroleum (Beijing) Strategic Cooperation Science and Technology Project (ZLZX2020-02), and Science Foundation of China University of Petroleum Beijing (No. 2462020YXZZ028). Ke Xu gratefully acknowledges the financial support and funding provided by the National Natural Science Foundation of China under Grant (No. 12172010), and by the CNPC Research Institute of Petroleum Exploration and Development for the project "Key Fluid Mechanisms of CO_2-EOR for Gu-Long Shale Oil Development". Special thanks to Changqing Oilfield for providing tight cores, crude oil and other important data.

Appendix A

The CT Scanning instrument used in this experiment consists of an X-ray computed tomography (X-CT) system and a core displacement system, as shown in Fig. A-1. The X-CT system is mainly composed of three parts, including a computer system, a CT scanner, and an image storage and display system. The computer system calculates and stores the data obtained by scanning the tomography of an object. The CT scanner mainly scans objects on the movable platform by emitting X-ray. The X-ray can penetrate non-metallic materials, and its wavelength and the property of objects will lead to different experimental data. The image storage and display system displays the reconstructed CT image processed by the computer system, which can be a 2D image or a 3D image.

The core displacement system is located on the movable platform, including injection pumps, a confining pressure pump, a backpressure pump, a core holder, and a pressure transducer. Two sets of injection pumps are used to inject crude oil and formation water, respectively. The special core holder shell is made of PEEK material that allows X-ray to pass through smoothly, thus reducing measurement error caused by the hardening effect of X-ray.

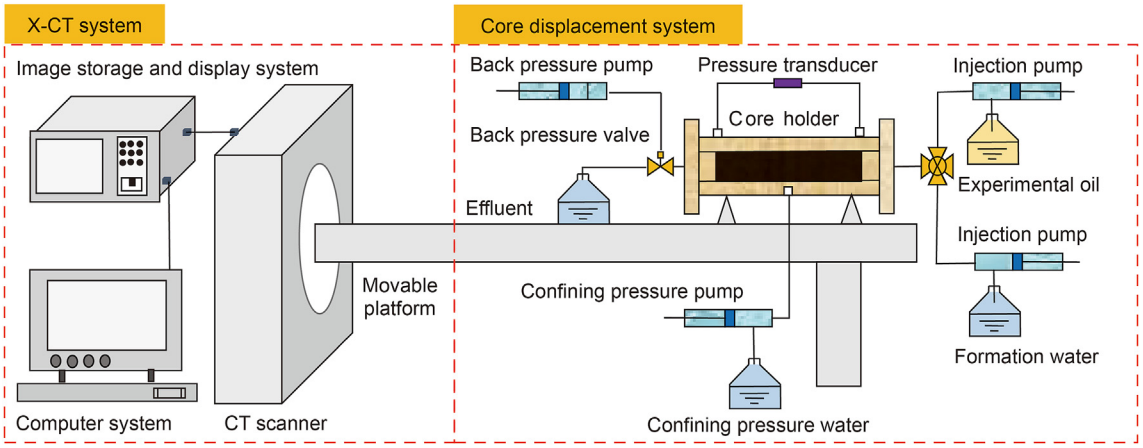

Fig. A-1. The schematic diagram of CT scanning instrument.

CT scanning technology can directly observe the distribution characteristics of two-phase fluid and extension of saturation profile in the core, which provides an intuitive basis for analyzing the front of water imbibition and determining CID. Assuming that the rock skeleton and pores are rigid bodies, the pores are completely saturated with formation water after vacuum treatment. During imbibition process, the pore structure and skeleton shape do not change, only fluid saturation in the pores changes. Our experiment follows the principle of substance conservation, and the volume of water entering the core is equal to the volume of oil produced from the core. According to the CT data of each cross-section, water saturation of each cross-section is calculated at different times for the core, as shown in Eq. A-1, and experimental measurement error of water saturation is 2%–3%. The error mainly comes from the experimental equipment and data processing, such as the positioning error of each scanning surface, the recognition accuracy of experimental equipment and the data processing error, etc.

$$S_w = \left(\frac{CT_{oil} - CT_{air}}{CT_{saturated} - CT_{dry}} \times \frac{CT_{imbibition} - CT_{saturated}}{CT_{water} - CT_{oil}} \right) \times 100\% \quad \text{(A-1)}$$

where CT_x is the CT value of x (x = air, oil, water, or dry core); $CT_{saturated}$ is the CT value of the core saturated with oil; $CT_{imbibition}$ is the CT value of core in imbibition process.

Appendix B

Capillary pressure curves of experimental core are shown in Fig. B-1. The characteristic parameters P_0 and b of each core can be obtained by fitting the experimental data, and fitting parameter results are shown in Table B-1. When other parameters are certain, capillary pressure is inversely proportional to the square root of permeability based on the Young-Laplace equation.

$$P_c = \frac{2\sigma\cos\theta}{r}$$

$$K = \frac{\phi r^2}{8\tau^2} \rightarrow P_c = \frac{\sigma\cos\theta}{\sqrt{2\tau}}\sqrt{\frac{\phi}{K}}.$$

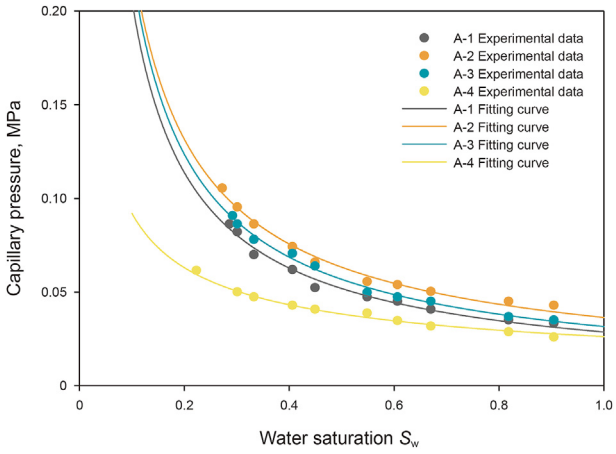

Fig. B-1. Experimental data and fitting results of capillary pressure curves.

Table B-1
Fitting parameter results of experimental cores.

Sample	P_0, MPa	b
A-1	0.030	1.2
A-2	0.038	1.3
A-3	0.031	1.18
A-4	0.0257	1.8

Referring to the experimental data of Lukyanov et al. (2012), the reasonable range of water-phase permeability under low saturation, i.e. kK_{rw}, can be calculated by Darcy formula ($q = -\frac{kK_{rw}}{\mu}\nabla P$). Then, through the Kozeny-Carman formula ($k = \frac{\phi r^2}{8\tau^2}$), the absolute permeability k can be approximatively calculated, and then K_{rw} can be obtained as the reference range of a. Finally, the reference interval of a is calculated as 1.10×10^{-4}–9.59×10^{-6}.

Incorporating Eqs. (9) and (10) into Eq. (8) can obtain the function expression $F(S)$ of the independent variable S, and then the expression of dF/dS can be obtained:

$$\frac{dF}{dS}=\frac{KP_0(S^n-1)(b+1)(S-1)^2(a+S^m)}{b^2\phi S^{\frac{b+1}{b}+1}z}-\frac{KP_0(S^n-1)(S-1)^2(a+S^m)\left[\mu_w(2S-2)(S^n-1)-mS^{m-1}\mu_o+nS^{n-1}\mu_w(S-1)^2\right]}{b\phi S^{\frac{b+1}{b}}z^2}$$
$$-\frac{KmP_0S^{m-1}(S^n-1)(S-1)^2+KP_0(2S-2)(S^n-1)(a+S^m)+KnP_0S^{n-1}(S-1)^2(a+S^m)}{b\phi S^{\frac{b+1}{b}}z}$$

with

$$m=\frac{2+3b}{b}$$

$$n=\frac{2+b}{b}$$

$$z=\left[\mu_o(a+S^m)-\mu_w(S^n-1)(S-1)^2\right]$$

The sensitivity analysis of the function $F(S)$ and critical saturation affected by parameters a and b is shown in Fig. B-2.

Appendix C

We analysis the data from Liu and Sheng (2020), which echoes our experimental observation. Experimental results also show two countercurrent imbibition stages, and the double logarithm graph of CID against t for experimental data is plotted for further analysis as shown in Fig. C-1a: the evolutions of early-stage CID are hidden due to too few experimental data, while late-stage CID increases much slower than $t^{0.5}$. At the same time, it can be seen from the linear plotting oil recovery vs. $t^{0.5}$ that the early recovery curves of experiment 2–5 show "downwardly concave" shape (Fig. C-1b), which implies that the early countercurrent imbibition evolution may be faster than $t^{0.5}$. The transition time from super-diffusive and sub-diffusive is also very close to that in our experiment. Regrettably, their early-time data is so few that more convincing analysis is not applicable.

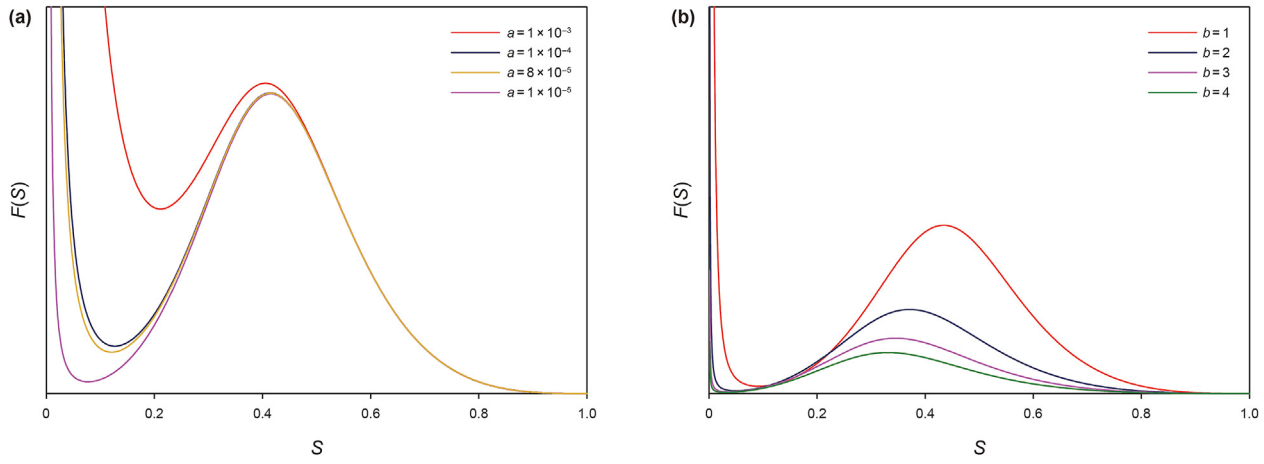

Fig. B-2. Change of transient time with parameter a and b. (**a**) Sensitivity analysis of parameter a (b = 1.2). (**b**) Sensitivity analysis of parameter b ($a = 10^{-5}$).

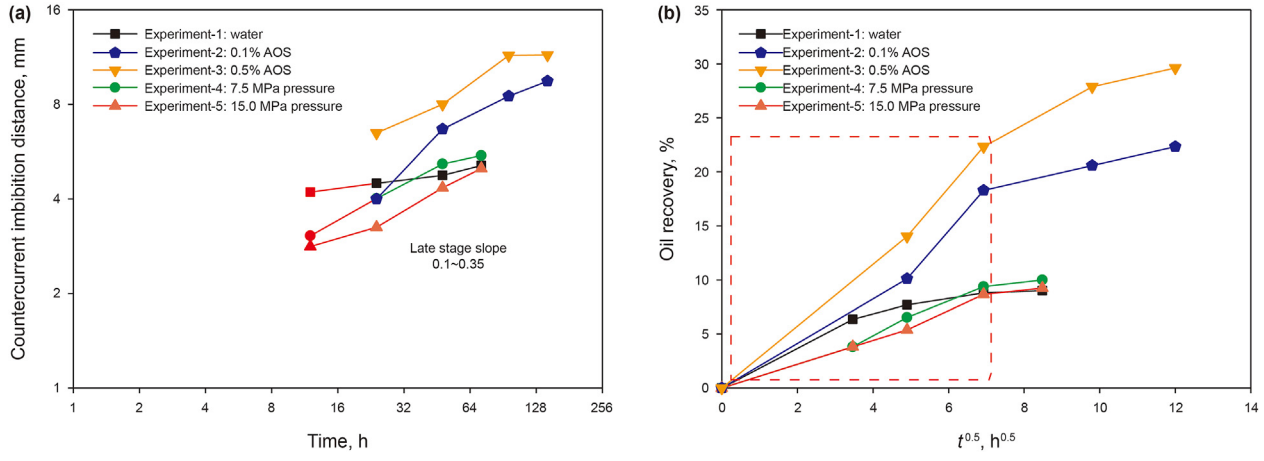

Fig. C-1. Replotted data of CID and time from Liu and Sheng (2020).

References

Barenblatt, G.I., 1971. Filtration of two nonmixing fluids in a homogeneous porous medium. Fluid Dynam. 6 (5), 857–864. https://doi.org/10.1007/BF01013869.

Barenblatt, G.I., Vinnichenko, A.P., 1980. Non-equilibrium seepage of immiscible fluids. Adv. Mech 3 (3), 35–50.

Bonn, D., Eggers, J., Indekeu, J., et al., 2009. Wetting and spreading. Rev. Mod. Phys. 81 (2), 739–805. https://doi.org/10.1103/RevModPhys.81.739.

Bourbiaux, B.J., Kalaydjian, F.J., 1990. Experimental study of cocurrent and countercurrent flows in natural porous media. SPE Reservoir Eng. 5 (3), 361–368. https://doi.org/10.2118/18283-PA.

Brooks, R.H., Corey, A.T., 1964. Properties of porous media affecting fluid flow. J. Irrig. Drain. Divis. Proceed. Am. Soc. Civil Eng. 92 (2), 61–88. https://doi.org/10.1061/JRCEA4.0000425.

Cao, C., Jia, P., Cheng, L., et al., 2022. A review on application of data-driven models in hydrocarbon production forecast. J. Petrol. Sci. Eng. 212, 110296. https://doi.org/10.1016/j.petrol.2022.110296.

Deng, L., King, M., 2019. Theoretical investigation of the transition from spontaneous to forced imbibition. SPE J. 24 (1), 215–229. https://doi.org/10.2118/190309-PA.

Fischer, H., Wo, S., Morrow, N.R., 2008. Modeling the effect of viscosity ratio on spontaneous imbibition. SPE Reservoir Eval. Eng. 11, 577–589. https://doi.org/10.2118/102641-MS.

Føyen, T.L., Fernø, M.A., Brattekas, B., 2019. The effects of nonuniform wettability and heterogeneity on induction time and onset of spontaneous imbibition. SPE J. 24 (3), 1192–1200. https://doi.org/10.2118/190311-PA.

Gruener, S., Huber, P., 2019. Capillarity-driven oil flow in nanopores: Darcy scale analysis of Lucas–Washburn imbibition dynamics. Transport Porous Media 126, 599–614. https://doi.org/10.1007/s11242-018-1133-z.

Guen, S., Kovscek, A.R., 2006. Nonequilibrium effects during spontaneous imbibition. Transport Porous Media 63 (1), 127–146. https://doi.org/10.1007/s11242-005-3327-4.

Hammecker, C., Mertz, J.D., Fischer, C., et al., 1993. A geometrical model for numerical simulation of capillary imbibition in sedimentary rocks. Transport Porous Media 12, 125–141. https://doi.org/10.1007/BF00616976.

Hatiboglu, C.U., Babadagli, T., 2007. Oil recovery by counter-current spontaneous imbibition: effects of matrix shape factor, gravity, ift, oil viscosity, wettability, and rock type. J. Petrol. Sci. Eng. 59 (1–2), 106–122. https://doi.org/10.1016/j.petrol.2007.03.005.

Hatiboglu, C.U., Babadagli, T., 2008. Primary and secondary oil recovery from different-wettability rocks by countercurrent diffusion and spontaneous imbibition. SPE Reservoir Eval. Eng. 11 (2), 418–428. https://doi.org/10.2118/94120-MS.

Hatiboglu, C.U., Babadagli, T., 2010. Experimental and visual analysis of co- and counter-current spontaneous imbibition for different viscosity ratios, interfacial tensions, and wettabilities. J. Petrol. Sci. Eng. 70 (3–4), 214–228. https://doi.org/10.1016/j.petrol.2009.11.013.

Hou, B., Zhang, F., Wang, S., et al., 2022. Mechanisms of spontaneous imbibition and wettability reversal of sandstone cores by a novel imbibition agent. Energy Fuel. 36 (3), 1316–1325. https://doi.org/10.1021/acs.energyfuels.1c03489.

Jabbari, H., Afsari, K., Rabiei, M., et al., 2017. Thermally-induced wettability alteration from hot-water imbibition in naturally fractured reservoirs—Part 1: numerical model development & 1D models. Fuel 208, 682–691. https://doi.org/10.1016/j.fuel.2017.07.016.

Kashchiev, D., Firoozabadi, A., 2003. Analytical solutions for 1D countercurrent imbibition in water-wet media. SPE J. 8 (4), 401–408. https://doi.org/10.2118/87333-PA.

Kim, S., Moon, M.W., Kim, H.Y., 2021. Liquid spreading along nanostructured superhydrophilic lanes. Phy. Rev. Fluid. 6 (3), 034002. https://link.aps.org/doi/10.1103/PhysRevFluids.6.034002.

Li, Y., Morrow, N.R., Ruth, D., 2003. Similarity solution for linear counter-current spontaneous imbibition. J. Petrol. Sci. Eng. 39 (3–4), 309–326. https://doi.org/10.1016/S0920-4105(03)00071-8.

Liu, G., Zhang, M., Ridgway, C., et al., 2014. Pore wall rugosity: the role of extended wetting contact line length during spontaneous liquid imbibition in porous media. Colloid. Surf. A Physicochem. Eng. Aspect. 443, 286–295. https://doi.org/10.1016/j.colsurfa.2013.11.033.

Liu, J., Sheng, J.J., 2020. Investigation of countercurrent imbibition in oil-wet tight cores using NMR technology. SPE J. 25 (5), 2601–2614. https://doi.org/10.2118/201099-PA.

Lukyanov, A.V., Sushchikh, M.M., Baines, M.J., et al., 2012. Superfast nonlinear diffusion: capillary transport in particulate porous media. Phys. Rev. Lett. 109 (21), 214501. https://doi.org/10.1103/PhysRevLett.109.214501.

Lu, H., Xu, Y., Duan, C., et al., 2022. Experimental study on capillary imbibition of shale oil in nanochannels. Energy Fuel. 36 (10), 5267–5275. https://doi.org/10.1021/acs.energyfuels.2c00309.

Masalmeh, S.K., Shiekah, I.A., Jing, X.D., 2007. Improved characterization and modeling of capillary transition zones in carbonate reservoirs. SPE Reservoir Eval. Eng. 10 (2), 191–204. https://doi.org/10.2118/109094-PA.

Mason, G., Fischer, H., Morrow, N.R., et al., 2009. Spontaneous counter-current imbibition into core samples with all faces open. Transport Porous Media 78 (2), 199–216. https://doi.org/10.1007/s11242-008-9296-7.

Mason, G., Fischer, H., Morrow, N.R., et al., 2010. Correlation for the effect of fluid viscosities on counter-current spontaneous imbibition. J. Petrol. Sci. Eng. 72 (1–2), 195–205. https://doi.org/10.1016/j.petrol.2010.03.017.

McWhorter, D.B., Sunada, K.D., 1990. Exact integral solution for two-phase flow. Water Resour. Res. 26 (3), 339–413. https://doi.org/10.1029/WR026i003p00399.

Meng, H., Bi, H.B., Duan, X.W., et al., 2018. Permeability indexes for defining tight oil reservoirs. In: ECMOR XVI-16th European Conference on the Mathematics of Oil Recovery. https://doi.org/10.3997/2214-4609.201802206.

Meng, Q., Cai, J., Wang, J., 2019a. Scaling of countercurrent imbibition in 2D matrix blocks with different boundary conditions. SPE J. 24 (3), 1179–1191. https://doi.org/10.2118/194207-PA.

Meng, Q., Cai, Z., Cai, J., et al., 2019b. Oil recovery by spontaneous imbibition from partially water-covered matrix blocks with different boundary conditions. J. Petrol. Sci. Eng. 172, 454–464. https://doi.org/10.1016/j.petrol.2018.09.075.

Meng, Q., Liu, H., Jing, W., 2017. Effect of viscosity on oil production by cocurrent and countercurrent imbibition from cores with two ends open. SPE Reservoir Eval. Eng. 20 (2), 251–259. https://doi.org/10.2118/183635-PA.

Mirzaei, M., Dicarlo, D.A., Pope, G.A., 2016. Visualization and analysis of surfactant imbibition into oil-wet fractured cores. SPE J. 21 (1), 101–111. https://doi.org/10.2118/166129-PA.

Polat, C., 2021. Insights into the solution of counter-current spontaneous imbibition for tight unconventional reservoirs. J. Petrol. Sci. Eng. 201 (8), 108505. https://doi.org/10.1016/j.petrol.2021.108505.

Pooladi-Darvish, M., Firoozabadi, A., 2000. Cocurrent and countercurrent imbibition in a water-wet matrix block. SPE J. 5 (1), 3–11. https://doi.org/10.2118/38443-PA.

Quere, D., 2008. Wetting and roughness. Annu. Rev. Mater. Res. 38 (1), 71–99. https://doi.org/10.1146/annurev.matsci.38.060407.132434.

Reis, J.C., Cil, M., 1993. A model for oil expulsion by counter-current water imbibition in rocks: one-dimensional geometry. J. Petrol. Sci. Eng. 10 (2), 97–107. https://doi.org/10.1016/0920-4105(93)90034-C.

Schmid, K., Alyafei, N., Geiger, S., et al., 2016. Analytical solutions for spontaneous imbibition: fractional-flow theory and experimental analysis. SPE J. 21 (6), 2308–2316. https://doi.org/10.2118/184393-PA.

Seyyedi, M., Sohrabi, M., 2015. Enhancing water imbibition rate and oil recovery by carbonated water in carbonate and sandstone rocks. Energy Fuel. 30 (1), 285–293. https://doi.org/10.1021/acs.energyfuels.5b02644.

Silin, D., Patzek, T., 2004. On barenblatt's model of spontaneous countercurrent imbibition. Transport Porous Media 54, 297–322. https://doi.org/10.1023/B:TIPM.0000003678.85526.b1.

Song, X., Zhao, M., Dai, C., et al., 2021. Mechanism of active silica nanofluids based on interface-regulated effect during spontaneous imbibition. Petrol. Sci. 18 (3), 883–894. https://10.1007/s12182-020-00537-8.

Standnes, D.C., Andersen, P.O., 2017. Analysis of the impact of fluid viscosities on the rate of countercurrent spontaneous imbibition. Energy Fuel. 31 (7), 6928–6940. https://doi.org/10.1021/acs.energyfuels.7b00863.

Tang, M., Wang, C., Deng, X., et al., 2022. Experimental investigation on plugging performance of nanospheres in low-permeability reservoir with bottom water. Adv. Geo-Energy Res. 6 (2), 95–103. https://doi.org/10.46690/ager.2022.02.02.

Tian, W., Wu, K., Gao, Y., et al., 2021. A critical review of enhanced oil recovery by imbibition: theory and practice. Energy Fuel. 35, 5643–5670. https://doi.org/10.1021/acs.energyfuels.1c00199.

U.S. Energy Information Administration (EIA), 2018. Annual Energy Outlook 2018. U.S. Energy Information Administration, 15 September, 2018. https://www.eia.gov/outlooks/aeo/.

U.S. Energy Information Administration (EIA), 2019. U.S. Crude Oil and Natural Gas Proved Reserves, Year-End 2019. U.S. Energy Information Administration. 11 January, p. 2021. https://www.eia.gov/naturalgas/.

Vazquez, J.L., 2006. Smoothing and Decay Estimates for Nonlinear Diffusion Equations—Equations of Porous Medium Type. Oxford University Press, New York.

Velasco-Lozano, M., Balhoff, M.T., 2021. A semi-analytical solution for countercurrent spontaneous imbibition in water-wet fractured reservoirs. Transport Porous Media 138, 77–97. https://doi.org/10.1007/s11242-021-01591-5.

Wang, X., Peng, X., Zhang, S., et al., 2018. Characteristics of oil distributions in forced and spontaneous imbibition of tight oil reservoir. Fuel 224, 280–288. https://doi.org/10.1016/j.fuel.2018.03.104.

Wang, Y., Cheng, S., Zhang, K., et al., 2019. A comprehensive work flow to characterize waterflood-induced fracture by integrating real-time monitoring, formation test, and dynamic production analysis applied to Changqing Oilfield, China. SPE Reservoir Eval. Eng. 22 (2), 692–708. https://doi.org/10.2118/191370-PA.

Wang, Y., Xu, H., Yu, W., et al., 2011. Surfactant induced reservoir wettability alteration: recent theoretical and experimental advances in enhanced oil recovery. Petrol. Sci. 8, 463–476. https://doi.org/10.1007/s12182-011-0164-7.

Wei, C., Cheng, S., Wang, Y., et al., 2021. Practical pressure-transient analysis solutions for a well intercepted by finite conductivity vertical fracture in naturally fractured reservoirs. J. Petrol. Sci. Eng. 204, 108768. https://doi.org/10.1016/j.petrol.2021.108768.

Xu, G., Han, Y., Jiang, Y., et al., 2021. Reducing residual oil saturation: underlying mechanism of imbibition in oil recovery enhancement of tight reservoir. SPE J. 26, 2340–2351. https://doi.org/10.2118/205491-PA.

Yang, L., Zhao, Y., Jiang, R., et al., 2019. Spontaneous capillary imbibition model in tight oil reservoirs. Mech. Eng. 41 (4), 398–404 (in Chinese).

Yang, S., Dehghanpour, H., Binazadeh, M., et al., 2016. A molecular dynamics explanation for fast imbibition of oil in organic tight rocks. Fuel 190, 409–419. https://doi.org/10.1016/j.fuel.2016.10.105.

Yang, Z., Liu, X., Li, H., et al., 2019. Analysis on the influencing factors of imbibition and the effect evaluation of imbibition in tight reservoirs. Petrol. Explor. Dev. 46 (4), 739–745. https://doi.org/10.1016/S1876-3804(19)60235-1.
Yu, F., Gao, Z., Zhu, W., et al., 2021. Experiments on imbibition mechanisms of fractured reservoirs by microfluidic chips. Petrol. Explor. Dev. 48 (5), 1004–1013. https://doi.org/10.1016/S1876-3804(21)60099-X.
Yu, H., Rui, Z., Chen, Z., et al., 2019a. Feasibility study of improved unconventional reservoir performance with carbonated water and surfactant. Energy 182, 135–147. https://doi.org/10.1016/j.energy.2019.06.024.
Yu, H., Yang, Z., Luo, L., et al., 2019b. Application of cumulative-in-situ-injection production technology to supplement hydrocarbon recovery among fractured tight oil reservoirs: a case study in Changqing Oilfield, China. Fuel 242, 804–818. https://doi.org/10.1016/j.fuel.2018.12.121.
Zhang, X., Morrow, N.R., Ma, S., 1996. Experimental verification of a modified scaling group for spontaneous imbibition. SPE Reservoir Eval. Eng. 11 (4), 280–285. https://doi.org/10.2118/30762-PA.
Zhou, D., Jia, L., Kamath, J., et al., 2002. Scaling of counter-current imbibition processes in low-permeability porous media. J. Petrol. Sci. Eng. 33 (1–3), 61–74. https://doi.org/10.1016/S0920-4105(01)00176-0.
Zou, C., Zhu, R., Li, J., et al., 2017. Geological Evaluating Methods for Tight Oil. GB/T 34906-2017. China Standards Press, Beijing.